PCCP

Accepted Manuscript

ROYAL SOCIETY OF CHEMISTRY

www.rsc.org/pccp

Quantum phase transitions in Sn bilayer based interfacial systems by external strain

Li Chen,[*,a] Qiandong Zhuang,[b] Yeqing Chen,[a] Changmin Shi,[a] and Dongchao Wang[b]

[a] *Institute of Condensed Matter Physics, Linyi University, Linyi 276005, People's Republic of China.*

[b] *Physics Department, Lancaster University, Lancaster LA1 4YB, UK.*

PACS number(s): 68.35.Gy, 73.20.At

Using the first-principle calculations, we report for the first time, the changes of electronic structures of a single bilayer Sn stacked on a single bilayer Sb (Bi) and on a single quintuple layer Sb_2Te_3 induced by both interface polarization and strain. With BL Bi and QL Sb_2Te_3 substrates, the stanene tends to have a low-buckled configuration, whereas with BL Sb substrate, the stanene prefers to form high-buckled configuration. For strained Sn/Sb (Bi) system, we find the Dirac cone state does not present in the band gap, while in strained Sn/Sb_2Te_3 system, spin-polarized Dirac cone can be introduced in the band gap. We discuss why tensile strain can result in Dirac cone emerging at K point based on a tight-binding lattice model. This theoretical study implies the feasibility of realizing quantum phase transitions for Sn thin films on suitable substrates. Our findings provide an effective manner in manipulating electronic structures and topological states in interfacial systems by use of interface polarization and strain, which opens a new route for realizing atomically thin spintronic devices.

Introduction

Exploring novel quantum phases has been a central issue of condensed matter physics and material science for decades. The interplay among orbital, charge and spin degree of freedom at nanoheterostructure offers an efficient way to generate and manipulate various quantum phases. The research became a most topical area in materials physics due to the recent development of the synthesis of controlled nanostructures, heterostructures and interfaces of semiconductors, metal–molecule–metal junction,[1] transition metal oxides and topological insulators. Thin films are often made by epitaxial growth on a substrate, where interface polarization and strain due to lattice mismatch and chemical heterogeneity between the film and the substrate are unavoidable. Strain and interfacial electrical field induced by interfacial charge transfer could significantly affect the electronic structures of interfacial systems.[2-8] The strain of interfacial systems was suggested to play an important role in modulating the degree of many-body interaction of topological band states and internal electrical field effect.[9–11] The interfacial electrical field and external strain are expected to affect the fundamental properties of systems, and conversely can be used as effective means to tailor the properties of materials for potential applications.

Stanene, whose high carrier mobility can be comparable to that of graphene, has been theoretically proposed to be a topological insulator (TI) with a relatively large bulk band energy gap of 0.1 eV,[12] which is promising for the realization of TI-based devices. Moreover, α-Sn under strain has been proposed as a 3D TI,[13] and epitaxial α-Sn has been successfully grown on InSb (001) substrates.[14,15] Tin (Sn) atoms bind to the gold support through strong chemical bonds where significant electronic charge transfer occurs from Sn to the gold support.[16] Remarkably, for a layer of Sn atoms, while a buckled structure is preferred in the free state, a planar graphene-like atomic arrangement is favorably stabilized on gold support. This structural change corroborates the metal-like band structure of the planar stanene in comparison to the semi-metallic buckled configuration. In addition, Sn and related two dimensional materials have stable phase structures and hydrophobic and antioxydant effects.[17-19] Very recently, the ultrathin Sn films with 2D stanene structure on the substrate of Bi_2Te_3

have been successfully grown.[20] The hole pockets of stanene observed experimentally at the Γ point, with the help of the Rashba effect due to the breaking of the inversion symmetry on the substrate, could potentially support topological superconductivity.[21] However, up to date, there is lack of study of the effects of interfacial polarization and strain on the electronic structure of Sn bilayers (BL), especially, a single Sn BL on Sb (Bi) BL or Sb_2Te_3 quintuple layer (QL).

Based on first-principles calculations, here we report the quantum phase transitions in interfacing systems consisting of two gapped Sn/Sb(Bi) (1BL Sn on 1BL Sb or Bi) and Sn/Sb_2Te_3 (1BL Sn on 1QL Sb_2Te_3) with ordinary fermions driven by interfacial electrical field and external strain. We found that interface polarization of Sn/Sb_2Te_3 system is smaller than that of Sn/Sb(Bi) system. Utilizing strain on Sn/Sb_2Te_3, the quantum phase transition can be tuned in Sn/Sb_2Te_3 system. In particular, a spin-polarized Dirac cones at K point inside band gap can be created as the strain increases to 4.3%. We discuss why tensile strain can result in Dirac cone emerging at K point based on a tight-binding lattice model. This theoretical work implies that quantum phase transitions in interfacing two gapped systems can be driven by interface polarization and strain, which provide new insight in future experimental studies as well as potential applications in spintronic and atomically thin circuitry.

Methods and parameters

A single BL stanene and 1 QL Sb (Bi) or Sb_2Te_3 are accumulated from top to bottom, e.g. Sn/Sb(Bi) or Sn/Sb_2Te_3, as shown in Fig. 1(a)-(c). The rhombus shows the unit cell. The blue, orange and green spheres indicate Sn, Sb(Bi) and Te atoms, respectively. The electronic band structures and the electronic properties of the interfacial Sn/Sb(Bi) (or Sn/Sb_2Te_3) system were calculated based on the framework of the Perdew–Burke–Ernzerhof (PBE)-type generalized gradient approximation using Vienna Ab initio Simulation Package (VASP),[22] as previously used for the calculations for graphene,[23,24] All calculations were performed with a plane-wave

cutoff of 400 eV on a 15 × 15× 1 Monkhorst-Pack k-point mesh. For structural relaxation, all the atoms are allowed to relax until atomic forces are smaller than 0.01 eV/Å. In our study, the direction of the z was chosen to be perpendicular to Sn/Sb(Bi) or Sn/Sb_2Te_3 film, and the vacuum layer is ~15 Å thick. The spin orbit coupling (SOC) was included in the self-consistent electronic structure calculations. The interfacial energy was calculated from a formula

$$E_{inter} = E_{total} - E_{Sn} - E_{substrate} \quad (1)$$

Where the $E_{inter.}$, E_{total}, E_{Sn} and $E_{substrate}$ is the interfacial energy, total energy of system, energy of Sn film and substrate such as Sb, Bi and Sb_2Te_3 films, respectively.

Results and discussion

The free standing 1BL Sn has a buckled honeycomb lattice with two atoms in primitive cell. There are two stable configurations: the high-buckled (HB) and low-buckled (LB) phase. HB phase is more stable than LB tin compatible with E_{LB}–E_{HB} = 0.24 eV, which is agreement with 0.25 eV in previous work.[25] The optimized lattice constants a_{HB} and a_{LB} are 3.41 Å and 4.67 Å for HB and LB phase, which is less and larger than that of BL Sb (4.12 Å), BL Bi (4.36 Å), and QL Sb_2Te_3 (4.32 Å),[26,27] respectively. Because of strong interaction between stanene and the substrates, the structural deformation will be induced after fully structural optimization, leading to different equilibrium lattice constant and buckled height. The optimized lattice constant is 4.03, 4.50 and 4.37 Å for Sn/Sb, Sn/Bi and Sn/Sb_2Te_3 systems, respectively. As discussed in previous work,[25] a transition among LB and HB structures occurs around $a = 1.2a_{HB}$. By checking the lattice parameters of equilibrium structures, we find that the buckled heights are 0.86 Å, 2.00 Å, 1.16 Å and 1.33 Å for free-standing LB stanene, stanene on BL Sb, Bi and QL Sb_2Te_3 substrates, respectively. With BL Bi and QL Sb_2Te_3 substrates, the stanene tends to have LB configuration, whereas with BL Sb, the stanene prefers to form HB configuration. It can be ascribed to the stronger interaction between stanene and BL Sb, because the interlayer distance (interface energy) between stanene and BL Sb is less (larger) than those between stanene and BL

Bi(and QL Sb_2Te_3)，which leads to the HB Sn and then Sn/Sb system is stable correspondingly.

The HB phase of BL Sn is metallic, while LB phase is with band gap depicted in Figure 1(d). It can be seen that the conduction band minimum (CBM) and the valence band maximum (VBM) lie exactly at K point. There is a direct band gap of 0.07 eV around the K point which is in agreement with previously calculated values.[12] We also checked the orbital components of the CBM and VBM coming from *p* orbitals. Two gapped single BL Sn and Sb films with an energy gap of 0.07 eV and 1.32 eV[26] respectively are formed in this interfacial Sn/Sb system. Figure 1(e) shows the band structure of interfacial Sn/Sb system with the optimized lattice constant a = 4.03Å, which exhibits a clear metallic Rashba state. The bands resulting mainly from Sn and Sb atoms are presented as red and blue color, respectively. At equilibrium, the interfacial distance d between Sn BL and Sb BL is 2.32Å and the interface energy is 0.47 eV per unit cell. These are noticeably larger than the typical values of chemical bond, but smaller than those of typical van der Waals bond. Consequently, the energy-degenerated states are split in the interfacial system. Similarly, a metallic Rashba state is presented in Figure 1(f) for the band structure of interfacial Sn/Bi system with the optimized lattice constant a = 4.50Å. The bands in red color and blue color mainly come from Sn and Bi atoms, respectively. At equilibrium, the interfacial distance d between Sn BL and Bi BL is 2.50Å and the interface energy is 0.31 eV per unit cell, which is less than that of Sn/Sb system. This explains why the band structure changes less than that of Sn/Sb system. There is a newly created Dirac point which is along the Γ-K direction. Unfortunately, the newly created Dirac point mentioned above are submerged in the “bulk” energy bands, which indicates that Dirac cone could not be observed by combining the Hall transport measurements and surface quantum control.

Figure 2(a) shows the band structure of interfacial Sn/Sb_2Te_3 system with the optimized lattice constant a = 4.37Å. It exhibits clearly a metallic Rashba state same as other systems. The bands in red color and blue colors indicate the major contribution of Sn BL and Sb_2Te_3 QL, respectively. At equilibrium, the interfacial

distance d between Sn BL and Sb_2Te_3 QL is 2.60Å and the interface energy is 0.25 eV per unit cell which are noticeably smaller than that of both Sn/Sb and Sn/Bi system. It is obvious that increasing interfacial distance and/or decreasing interfacial coupling in Sn/Sb_2Te_3 system induce less change in reshaped bands and Rashba splitting. This is because that the Rashba splitting is proportional to the interfacial coupling. One sees that the original CBM and VBM at the K point move below the Fermi level, so that the band gap is closed with the interfacial coupling. Another interesting feature is that the band splitting results effectively in the formation of Dirac bands with almost linear dispersion around Γ point. This is in a good agreement with the results reported in ref. 9. It is worthy noting that the newly created Dirac points are also submerged in the "bulk" energy bands. This indicates that the Dirac cone could not be observed by surface quantum control. It hopes to tune helical Dirac points being in the gap of bulk bands, so that Rashba states and consequently their peculiar properties may be accessed.

It should be noted that there are other factors could affect the properties of interfacial systems, for instance, epitaxial strain, structural deformation, molecular orbital hybridization, electron-phonon interaction and interfacial charge transfer etc. Amongst these factors, the strain and interfacial electrical field induced by interfacial charge transfer were proposed to offer significant effects to the electronic structures of interfacial systems.[7, 26] Thus, strain and charge transfer are the two most important extrinsic factors to engineering the intrinsic properties of Sn/Sb_2Te_3 system. It is anticipated that introducing tensile biaxial strain will tune helical Dirac points existing in the gap of bulk bands. One found that two bands around Fermi level at K coming from Sn nearly cross with increasing tensile biaxial strain seen from Fig. 2(b) with tensile biaxial strain 1.8%. Under strain of 4.3% (with lattice constant a = 4.56 Å), the BL-QL distance increases to 2.90 Å with a decreased interface energy of 0.17 eV. The increased BL-QL distance and the decreased interface energy reduce the BL-QL coupling. Figures 2(c) and its the enlarged view Fig. 2(d) show the typical band structures of Sn/Sb_2Te_3 system under tensile biaxial strain (4.3%) where the red and blue colors present the contribution of Sn BL and Sb_2Te_3 QL, respectively. Under

tensile strain, the position of VBM and CBM move to the Fermi level and connect at K point, forming a spin-polarized Dirac cone inside the "bulk" band gap. Therefore, Rashba states and their peculiar properties could be accessed by quantum control. We should emphasize that the interfacial coupling plays an important role to induce the Dirac cone. Based on the analysis of separated band structures for Sn BL and Sb_2Te_3 QL in Sn/Sb_2Te_3 system as shown in Fig. 3(a) and (b), and compared with the free standing band structures of 1BL Sn(111) (c) and (d) 1QL Sn_2Te_3 with a = 4.56Å, respectively, one can convince that the strained bands do not present the Dirac cone independently. Coupled with the help of the Rashba effect due to the breaking of the inversion symmetry on the substrate, the Dirac cone emerges inside the "bulk" band gap.

Dirac state is characterized by the spin-momentum locking relations:[28] (i) the spin direction is perpendicular to the momentum direction; (ii) the spins have the opposite directions at the inverse momenta. Next, we should confirm the helical properties of strained (under 4.3% strain with a = 4.56 Å) Sn/Sb_2Te_3 system when the inversion symmetry is broken by interface polarization. Note that for the valence bands as shown in Fig. 4(a), the in-plane spin projections within kx (ky) ~ 0.75-0.84 (2π/a) $Å^{-1}$ shows clockwise rotation around the K point. The solid line shows the energy contour. The spin texture for the conduction bands is plotted in Fig. 4(b), which shows counterclockwise rotation around the K point. It should be noted that the spin directions of the spin-split states can be changed by interface polarization, but the rotations of spins around the K point in conduction bands above Fermi level and in valence bands below Fermi level are still along opposite directions. There is no doubt that the spins are in opposite directions at the inverse momenta.

It is of importance to understand the interfacial interactional mechanism. The differential charge density at the interface is defined as

$$\rho = \rho_{Sn/Sb_2Te_3} - \rho_{Sn} - \rho_{Sb_2Te_3} \quad (2)$$

where ρ_{Sn/Sb_2Te_3}, ρ_{Sn}, and $\rho_{Sb_2Te_3}$ are the charge density of Sn/Sb_2Te_3, 1BL Sn and 1QL Sn_2Te_3 at the same 2D lattice constant without strain. As can be seen in Fig.

4(c)-(d), the BL Sn acts as a donor and the Sb_2Te_3 acts as an acceptor, with the electrons transferring from the Sn to the Sb_2Te_3. This charge transfer generates a large internal electric field which is estimated up to ~1V/Å at the interface region, with a field direction pointing from the Sn BL to the Sb_2Te_3 QL. Under tensile biaxial strain of 4.3%, the QL Sb_2Te_3 substrate provides a possible triggering mechanism that induces the Dirac cone states in Sn BL, although Dirac cone states are originated in the Sn BL. There appears a Rashba effect resulting from the internal electrical field induced by interfacial charge transfer when the BL Sn is grown on Sb_2Te_3 substrate. Figure 4(e) and (f) shows the differential charge density at the interface for the strained system. Clearly, the charge transfer is less at the interface than that of un-strained system because the interface distance in the latter is larger and thus the interface coupling is relatively small. Therefore, there is band gap between VBM and CBM except K point.

Next, we will discuss why tensile strain can result in Dirac cone emerging at K point based on a tight-binding lattice model. With next-nearest-neighbor tight-binding lattice model, the low-energy effective Hamiltonian involving time-reversal-invariant spin-orbit interaction for the free standing LB Sn around the K point reads[29]

$$\begin{aligned} H_k^{eff}(\theta) &= H_k \otimes I_2 + H_{so}^{1st} + H_{so}^{2nd} + H_R \\ &= (\varepsilon_1 - \lambda_{so}^{2nd}) I_4 + \begin{pmatrix} h_{11} & v_F k_+ \\ v_F k_- & -h_{11} \end{pmatrix} \\ h_{11} &= -\lambda_{so}\sigma_z - a\lambda_R(k_y\sigma_x - k_x\sigma_y) \end{aligned} \tag{3}$$

where I_2 is the 2 × 2 identity matrix for the spin degree of freedom, I_4 is the 4 × 4 identity matrix, $\lambda_{so} = \lambda_{so}^{1st} + \lambda_{so}^{2nd}$,

$$\lambda_{so}^{1st} \approx \frac{\xi_0}{2}\frac{2}{9}\frac{\Delta^2(V_{pp\pi} - V_{pp\sigma})}{V_{sp\sigma}^4} \times \frac{cot^2\theta}{1 + \frac{cos^2\theta(V_{pp\pi} - V_{pp\sigma})^2}{V_{sp\sigma}^2}\left(1 + \frac{2}{9}\frac{\Delta^2}{sin^2\theta V_{sp\sigma}^2}\right)} \tag{4}$$

$$\lambda_{so}^{2nd} \approx \left(\frac{\xi_0}{2}\right)^2 \frac{2}{9}\frac{-\Delta}{sin^2\theta V_{sp\sigma}^2} \tag{5}$$

$$v_F = -\frac{\sqrt{3}}{2}a[u_{11}^2(V_{pp\pi}sin^2\theta + V_{pp\sigma}cos^2\theta) - u_{21}^2 V_{ss\sigma} + 2u_{11}u_{21}cos\theta V_{sp\sigma} - \frac{1}{2}|u_{31}|^2 sin^2\theta(V_{pp\sigma} - V_{pp\pi})],$$

$$k_+ = k_x + ik_y, \quad k_- = k_x - ik_y, \tag{6}$$

where u_{ij} is the matrix element of unitary transformation. H_R is the intrinsic Rashba SOC in stanene. $Vpp\pi$, $Vpp\sigma$, $Vss\sigma$ and $Vsp\sigma$ are bond parameters. The angle θ is between the Sn-Sn bond and the z direction. Where Δ is the energy difference between the 3*s* and 3*p* orbitals, ξ_0 is the strength of SOC. Equation (3) results in a spectrum

$$E(k) = \pm\sqrt{(v_F^2 + a^2\lambda_R^2)k^2 + \lambda_{SO}^2} \tag{7}$$

Therefore, the energy gap is $2\lambda_{so}$ at the K point. Due to the LB geometry, the first-order and second-order SOC λ_{so}^{1st} and λ_{so}^{2nd} are 29.9 and 34.5 meV, respectively. The band gap is 129 meV, which is comparing with 70 meV calculated (PBE) in our work. The smaller is the angle θ, the less is the direct gap at K point. In particular, the gap can reach several meV for just a little buckling. Therefore the Quantum Spin Hall Effect (QSHE) can be observed in an experimentally attainable temperature regime.

When the Sn BL is stacked on Sb_2Te_3 QL, extrinsic Rashba SOC may appear due to the broken mirror symmetry. At equilibrium, one can assume that the extrinsic Rashba SOC can be comparable to that of intrinsic SOC (9.5 meV). The extrinsic Rashba SOC due to a perpendicular interfacial electric field may be written as[30]

$$\lambda_R = \frac{eE_z z_0}{3V_{sp\sigma}}\xi_0 \tag{8}$$

where z_0 is proportional to the atomic size of stanene. Assuming an interfacial electric field E_z is ~1 V/ Å, z_0 is ~ 4.99a_B, and ξ_0 =0.8,[29] the magnitude can be deduced as about 5.22 meV. Under tensile strain, both the angle θ and z_0 decrease, leading to a reduced λ_{so} and extrinsic Rashba SOC λ_R. On the other hand, the strain-induced different Rashba states which originate from their different response to strain, can be understood from deformation potential theory.[31,32] The surface states is presented by defining the surface deformation potential,[33]

$$\Xi = \frac{\partial E_F}{\partial \varepsilon} \tag{8}$$

where E_F and ε represent Fermi energy and the applied strain, respectively. As Fermi energies of different strained systems are different, the deformation potential of the

band at K point with -13.78eV in Sn/Sb_2Te_3 system is smaller than -10.87 and -11.93eV in Sn/Sb and Sn/Bi interfacial systems, respectively. This indicates that the band of Sn/Sb_2Te_3 system is very sensitive to strain. So Sn/Sb_2Te_3 system is more superior and more practical than that in Sn/Sb and Sn/Bi interfacial systems to tune quantum phase with a spin-polarized Dirac cone at K point inside band gap under tensile strain. There have another reason to explain why strain could not induce the dirac point in Sn/Sb(Bi) system. From the band structures of Sn/Sb(Bi) in Fig1, we can see the bands around the Fermi level bend and split seriously due to strong interface interaction based on interface energy which are 0.47 and 0.31 eV for Sn/Sb and Sn/Bi system, respectively. To form the Dirac point with large strain in Sn/Sb(Bi) system may not be accessible experimentally at the current technology. In addition, large strain will lead to instability of interface systems. The Rashba bands as depicted in color at the K and Γ points are very sensitive to strain. Consequently, with the increasing tensile strain, the p_z orbitals of Sn at K point and $p_{x,y}$ orbitals of Sn at Γ point are both strengthened. As a result, the bands at the K and Γ points shifts upward and downward relative to Fermi level, respectively, which can be seen clearly in Fig. 2(c) and (d). More important, a Dirac cones at K point presents inside band gap at a critical strain of 4.3%. This calculation explains why quantum phase transition can be easily tuned in strained Sn/Sb_2Te_3 system (up to 4.3%) with a creation of a spin-polarized Dirac cones at K point inside band gap.

Conclusions

In conclusion, using first-principles calculations, we performed a systematic theoretical study of electronic properties of single BL Sn on Sb (Bi) and a single quintuple layer Sb_2Te_3 changes with interface polarization and strain. The charge transfer generates a large internal electric field up to ~1 V/Å. This interfacial electric field breaks the inversion symmetry of the system and consequently violently splits the spin degeneracy of bands. Our calculations demonstrate that the helical Dirac point can be created by introducing tensile strain under the condition of less interfacial coupling with substrates and lees deformation potential, corresponding LB

Sn on substrates. This study provides a deep insight of the effect of substrate and strain on stanene and experimental fabrication of stanene. In addition, due to the general nature of the approach, our conclusions are capable to be extended to other film on non-metallic surfaces.

Acknowledgments

We thank financial support from the National Natural Science Foundation of China (Grant Nos. 51431004, 11274151 and 51302262), from Key Disciplines of Condensed Matter Physics of Linyi University. L.C. conceived the study, performed the first-principles calculations, and wrote the manuscript. Q.Z. wrote the manuscript, Y. C., S. C. and D. W. performed the first-principles calculations and discussed about the study.

*Corresponding author: chenli@lyu.edu.cn

1 H. M. Liu, N. Wang, J. W. Zhao, Y. Guo, X. Yin, Freddy. Boey and H. Zhang, *Chem. Phys. Chem.* 2008, **9**, 1416.
2 D. Wu, M. G. Lagally and F. Liu, *Phys. Rev. Lett.*, 2011, **107**, 236101.
3 H. Hu, H. J. Gao and F. Liu, *Phys. Rev. Lett.* 2008, **101**, 216102.
4 Z. Liu, J. Wu, W. Duan, M. G. Lagally and F. Liu, *Phys. Rev. Lett.*,2010, **105**, 016802.
5 D. Yu, Y. Zhang and F. Liu, *Phys. Rev. B*, 2008, **78**, 245204.
6 D. Sander, S. Ouazi, A. Enders, Th. Gutjahr-Loser, V. S. Stepanyuk, D. I. Bazhanov and J. Kirschner, *J. Phys.: Condens. Matter*, 2002, **14**, 4165.
7 L. Chen, Z. F. Wang and F. Liu, *Phys. Rev. B*, 2013, **87**, 235420.
8 D. C. van der Laan and J. W. Ekin, *Appl. Phys. Lett.*, 2007, **90**, 052506.
9 Z. F. Wang, M. Y. Yao, W. Ming, L. Miao, F. Zhu, C. Liu, C. L. Gao, D. Qian, J. F. Jia and F. Liu, *Nat. Commun.*,2013, **4**, 1384.
10 T. Hirahara, N. Fukui, T. Shirasawa, M. Yamada, M. Aitani, H. Miyazaki, M. Matsunami, S. Kimura, T. Takahashi, S. Hasegawa and K. Kobayashi, *Phys. Rev. Lett.*, 2012, **109**, 227401.
11 L. Miao, Z. F. Wang, W. Ming, M. Y. Yao, M. X. Wang, F. Yang, F. Zhu, A. V. Fedorovc, Z. Sun, C. L. Gao, C. Liu, Q. K. Xue, C. X. Liu, F. Liu, D. Qian and J. F. Jia, *Proc. Natl. Acad. Sci. USA*, 2013, **110**, 2758.
12 Y. Xu, B. Yan, H.-Jun Zhang, J. Wang, G. Xu, P. Tang, W. Duan, and S. C. Zhang, *Phys. Rev. Lett.*, 2013, **111**, 136804.
13 L. Fu and C. L. Kane, *Phys. Rev. B*, 2007, **76**, 045302.
14 Y. Ohtsubo, P. Le F`evre, F. Bertran, and A. Taleb-Ibrahimi, *Phys. Rev. Lett*., 2013, **111**,216401.
15 A. Barfuss, L. Dudy, M. R. Scholz, H. Roth, P. H¨opfner, C. Blumenstein, G. Landolt, J. H. Dil, N. C. Plumb, M. Radovic, A. Bostwick, E. Rotenberg, A. Fleszar, G. Bihlmayer, D. Wortmann, G. Li, W. Hanke, R. Claessen, and J. Sch¨afer, *Phys. Rev. Lett*. 2013, **111**, 157205.
16 S. Nigam, S. Gupta, D. Banyai, R. Pandey and C. Majumder, *Phys.Chem.Chem.Phys.*, 2015, **17**,6705 (2015).
17 L. Takahashi, and K.Takahashi. *Phys.Chem.Chem.Phys*., 2015, **17**, 21394.
18 K. Takahashi, and L. Takahashi. *Dalton Trans.*,2016, **45**, 3244.
19 C. J. Tong, H. Zhang, Y. N. Zhang, H. Liu and L. M. Liu. *J. Mater. Chem*. A, 2014, **2**, 17971.
20 F. F. Zhu, W. J. Chen, Y. Xu, C. L. Gao, D. D. Guan, C. H. Liu, D. Qian, S. C. Zhang and J. F. Jia, *Nat. Mater.*,2015, **14**, 1020.
21 J. Wang, Y. Xu and S. C. Zhang, *Phys. Rev. B*, 2014, **90**, 054503.
22 G. Kresse and J. Hafner, *Phys. Rev. B*, 1993, **47**, 558.
23 L. Chen, D. Yu and F. Liu, *Appl. Phys. Lett*.,2008, **93**, 223106.
24 L. Chen, H. Hu, Y. Ouyang, H. Z. Pan, Y. Y. Sun and F. Liu, *Carbon*, 2011, **49**, 3356.
25 P. Rivero, J. A. Yan, V´ıctor M. Garc´ıa-Su´arez, J. Ferrer and S. Barraza-Lopez, *Phys. Rev. B*, 2014, **90**, 241408(R).
26 D. C. Wang, Li Chen, H. M. Liu, X. L. Wang, G. L. Cui, P. H. Zhang, D. P. Zhao and S. H. Ji, *Phys. Chem. Chem. Phys*., 2015, **17**, 3577.
27 Z. F. Wang, L. Chen and F. Liu, *Nano Lett.*, 2014, **14**, 2879.
28 Y. H. Zhao, Y. B. Hu, L. Liu, Y. Zhu and H. Guo. *Nano Lett*., 2011, **11**, 2088.
29 C. C. Liu, H. Jiang and Y. G. Yao, *Phys. Rev. B*, 2011, **84**, 195430.
30 H. Min, J. E. Hill, N. A. Sinitsyn, B. R. Sahu, L. Kleinman and A. H. MacDonald,

Phys. Rev. B, 2006, **74**, 165310.

31 C. Herring and E. Vogt, *Phys. Rev.*, 1956, **101**, 944.

32 H. Hu, M. Liu, Z. F. Wang, J. Zhu, D.Wu, H. Ding, Z. Liu and F. Liu, *Phys. Rev. Lett*., 2012, **109**, 055501.

33 M. Zhou, Z. Liu, Z. F. Wang, Z. Q. Bai, Y. P. Feng, M. G. Lagally and F. Liu, *Phys. Rev. Lett*., 2013, **111**, 246801.

Figure captions

Fig. 1 (Color online) (a) Top view and (b) side view of the atomic structure of 1BL Sn on Sb (Bi), and (c) side view of the atomic structure of 1BL Sn on 1QL Sb_2Te_3. The rhombus shows the unit cell. The blue, orange and green spheres indicate Sn, Sb(Bi) and Te atoms, respectively. Band structures long Γ- K- M- Γdirections, (d) for 1BL free standing LB Sn film with optimized lattice constant a = 4.67Å, green, magenta, dark lines on the bands illustrate the contribution from p_x, p_y, and p_z states. (e) 1BL Sn on 1BL Sb with optimized lattice constant a = 4.03Å, the red and blue lines on the bands illustrate the contribution from Sn BL and Sb BL and (f) for 1BL Sn on 1BL Bi with optimized lattice constant a = 4.50Å, the red and blue lines on the bands illustrate the contribution from Sn BL and Bi BL, respectively.

Fig. 2 (Color online) Band structures of 1BL Sn(111) on 1QL Sn_2Te_3 along Γ- K-M- Γ directions under different strains, (a) tensile strain 0% with *a* = 4.37Å, (b) tensile strain 1.8% with a = 4.45Å, (c) tensile strain 4.3% with *a* = 4.56Å and (d) the enlarged view of (c), the red and blue lines on the bands illustrate the contribution from Sn BL and Sb_2Te_3 QL, respectively.

Fig. 3 (Color online) The "fat-bands" (green, magenta, dark) (a) derived from p_x, p_y, and p_z states of 1BL Sn(111), respectively, and (b) derived from p_x, p_y, and p_z states of 1QL Sb_2Te_3 layer in interfacial system, respectively. The free standing band structures of 1BL Sn(111) (c) and (b) 1QL Sn_2Te_3 with *a* = 4.56Å, green, magenta, dark lines on the bands illustrate the contribution from p_x, p_y, and p_z states, respectively.

Fig. 4 (Color online) Nontrivial Spin textures of the valence and conduction surface bands are shown in (a) and (b), respectively, for 1BL Sn on 1QL Sb_2Te_3 under 4.3% strain with *a* = 4.56 Å. The charge density isosurface in the internal electrical field is set to be 0.001 e /$Å^3$. Interfacial charge transfer between Sn BL and Sb_2Te_3 QL with a = 4.37 Å (c) and (d), a = 4.56 Å (e) and (f), as a function of the z coordinate perpendicular to the surface, showing the internal electrical field.

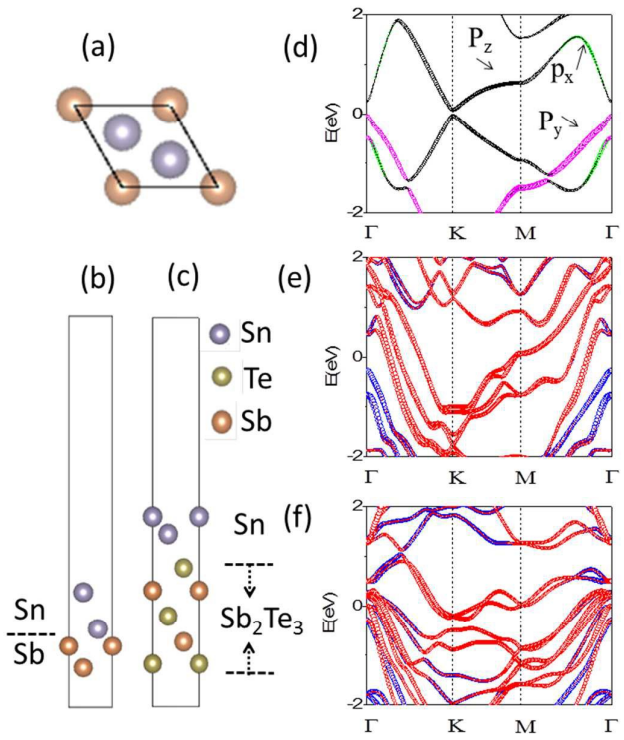

Fig.1/ Li Chen

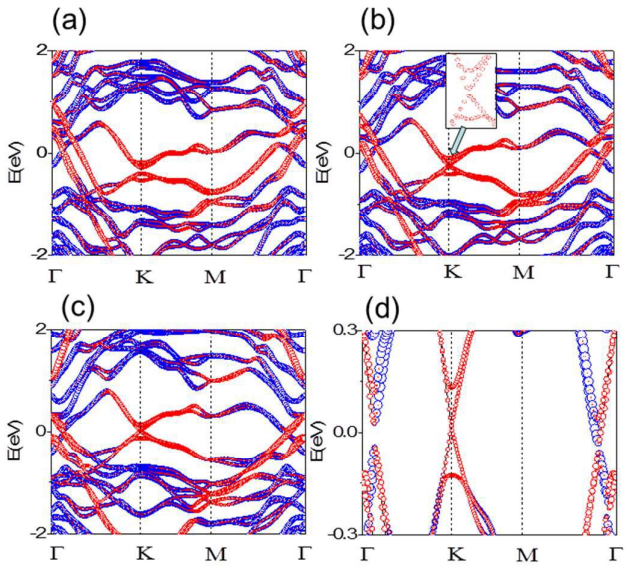

Fig.2/ Li Chen

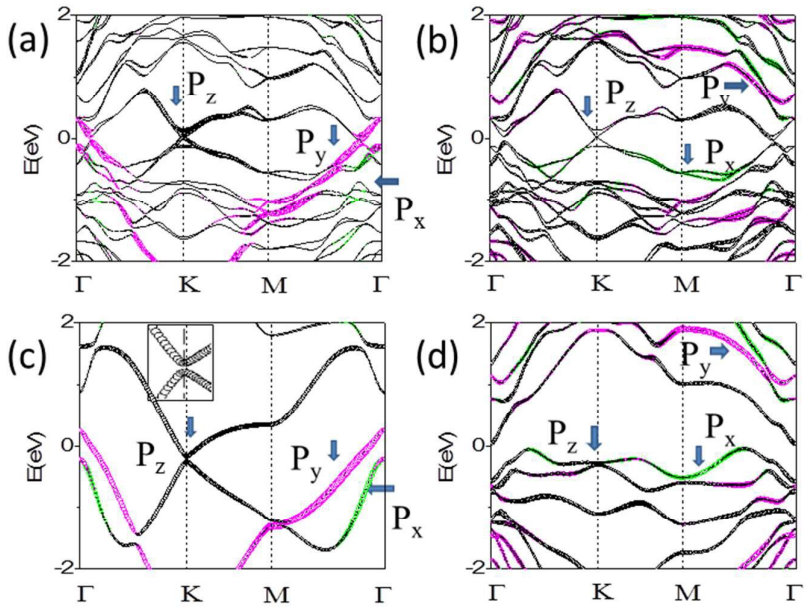

Fig.3/ Li Chen

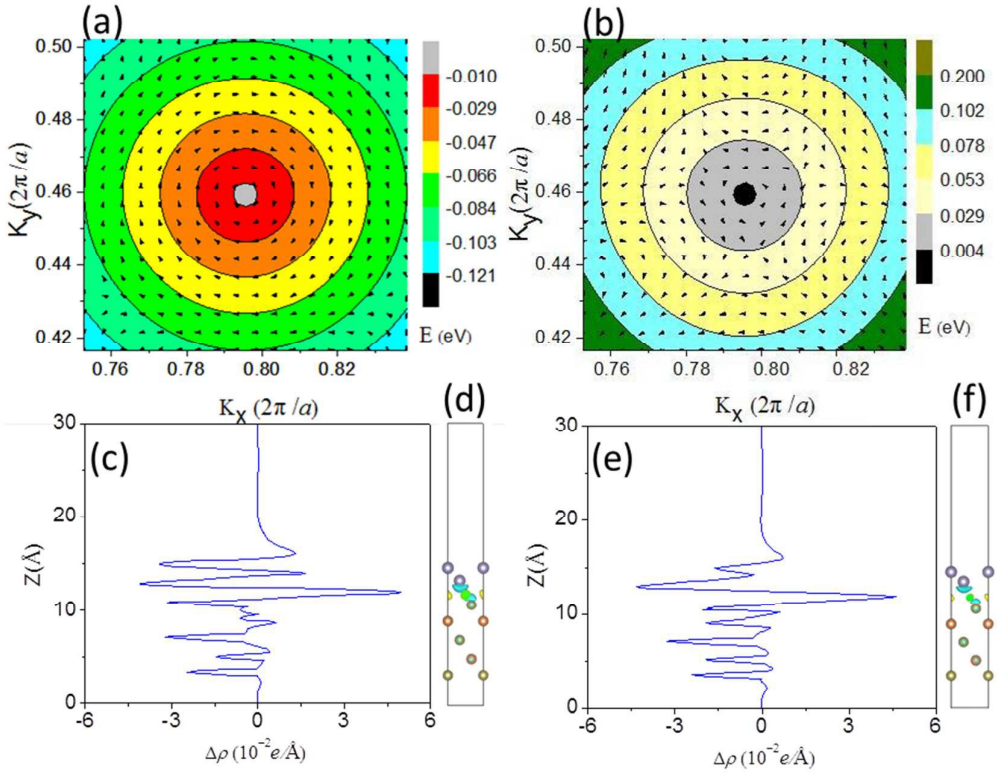

Fig.4/ Li Chen